NO_X emissions in West African cities inferred using TROPOMI NO_2 observations

AUTHOR NAMES: Madeline A. Miles[1], Aissatou Faye[1], Tahi P. Wiggins[1], Demba Ndao Niang[2], Mamadou S. Drame[2], Kang Sung[3,4], Sally E. Pusede[1]*

[1]Department of Environmental Sciences, University of Virginia, Charlottesville, VA 22904, USA

[2]Simeon Fongang Laboratory of Atmospheric Oceanic Physics, University of Cheikh Anta Diop

[3]Department of Civil, Structural and Environmental Engineering, University at Buffalo, Buffalo, New York

[4]Research and Education in eNergy, Environment and Water (RENEW) Institute, University at Buffalo, Buffalo, New York

*Corresponding author: sepusede@virginia.edu

ABSTRACT. Poor air quality is a growing issue in West African cities. Nitrogen oxides ($NO_x \equiv NO + NO_2$) play a key role in urban air pollution, affecting the atmospheric oxidation capacity and the production of other pollutants including ozone and secondary particulate matter. NO_x emissions in West African cities are uncertain, owing in part to the region's rapid urbanization, more diverse traffic and energy sources, and lack of surface monitoring. Here, we use observations from the TROPOspheric Monitoring Instrument (TROPOMI) to infer NO_x emission rates for 22 cities in West Africa. We use two established methods, exploiting the downwind decay of urban city plumes and manipulating flux divergence maps to estimate point sources. We compare the

two methods against inventory values, and we quantify and compare emissions in different cities separately on weekdays and Sundays. We advance the plume fitting method to study overlapping plumes, focusing on Dakar, Senegal, which is isolated from major cities, however is located adjacent to the large NO_x sources of the Industrial Zone and international airport. Prevailing north-south winds during the dry season allow for the distinction of the three overlapping plumes, and we test two methods of estimating individual source emissions.

INTRODUCTION

Urban air pollution is a growing issue in West Africa,[1, 2] with poor air quality contributing to a substantial portion of premature deaths in cities.[3, 4] Few places in the world are urbanizing as fast as West Africa, where cities are growing at a rate of almost 4% per year.[5] Because of the rapid pace of urbanization,[6] pollution sources are more diverse and uncontrolled than in cities in the U.S. and Europe, especially from fuel combustion and industrial sources.[7, 8] Regionally, vehicle pollution is exacerbated by the use of unregulated fuels, severe urban traffic congestion, and the import of older, more-polluting vehicles from the U.S., Europe, India, and China,[9-11] with local evidence suggesting that people who frequent areas with high traffic density are more likely to experience air pollution-related health impacts.[12]

Nitrogen dioxide (NO_2) is a combustion pollutant that plays a crucial role in the oxidative capacity of the atmosphere and the formation of other harmful pollutants such as ozone and secondary particulate matter. Emitted as NO_x ($\equiv$ NO + NO_2), major urban NO_2 sources include vehicle exhaust, fuel and waste burning, power generation, and industrial activities. Bahino et al.[8] compiled published NO_2 surface measurements in eight West African countries, with some cities reporting average NO_2 concentrations approaching or exceeding the World Health Organization (WHO) annual ambient standard of 40 $\mu g\ m^{-3}$ (21 ppb)[13, 14] and empirical evidence of much higher

43 urban levels on shorter-time scales.[13, 15-20] Comparison between cities is made difficult by the lack
44 of routine NO_2 surface monitoring,[8, 21] leading to large uncertainties in causes and consequences
45 of poor air quality across West African cities.

46 Satellites observe NO_2 spatial and temporal patterns, inter-urban differences, and NO_x source
47 contributions in the absence of surface measurements.[22-27] Recently, Hickman et al.[2] used NO_2
48 tropospheric vertical column densities (TVCDs) from the Ozone Monitoring Instrument (OMI) to
49 show that increases in urban NO_x emissions in West African cities have been at least partially
50 offset by declines in regional biomass burning. Because NO_2 has a short atmospheric lifetime,
51 elevated NO_2 concentrations are co-located with emission sources, with past research showing that
52 NO_x emission rates can be inferred for large urban areas by integrating NO_2 plume downwind
53 decay gradients or by obtaining NO_x emission maps from the NO_x flux divergence.[28-35] Higher
54 spatial resolution NO_2 observations have recently become available with the launch of the
55 Tropospheric Ozone Monitoring Instrument (TROPOMI), which has an order of magnitude
56 improved spatial resolution than OMI, facilitating research on controls over NO_2 pollution in
57 smaller cities and with reduced temporal averaging than previously possible.[31]

58 In this manuscript, we use TROPOMI NO_2 observations to calculate and compare NO_x emission
59 rates for 22 West African cities ranging in population between 35,000 and 9 million. We do this
60 based on two established methods, exploiting both urban plume downwind distance-decay rates[28]
61 and divergence maps of horizontal NO_2 fluxes.[35] We compare inferred annual fluxes to estimates
62 from the most recent version of the Emissions Database for Global Atmospheric Research
63 (EDGAR) v 5.0,[36] and separately analyze observations on timescales useful for the interpretation
64 of emissions variability, on weekdays (Tuesdays–Saturdays) and Sundays.. We present a detailed

comparison of NO_x emission estimates in Dakar, Senegal, expanding application of urban plume-based approach to account for NO_2 sources in close spatial proximity.

MEASUREMENTS AND METHODS

TROPOMI. The Tropospheric Ozone Monitoring Instrument (TROPOMI) detects a variety of atmospheric trace gases in the ultraviolet and visible (270–500 nm), near-infrared (675–775 nm), and shortwave infrared (2305–2385 nm) spectral regions. Onboard the sun-synchronous Copernicus Sentinel-5 Precursor satellite, TROPOMI collects measurements daily at ~1:30 pm local time (LT).[37, 38] NO_2 is retrieved by fitting the 405–465 nm band using an updated OMI DOMINO algorithm based on QA4ECV project.[39-43] The nadir spatial resolution of TROPOMI was originally 3.5 km x 7 km, but it was updated to 3.5 km x 5.5 km after 6 August 2019. TROPOMI has a documented low bias of 30–60% under high NO_2 conditions,[43, 44] with uncertainties dominated by the coarse resolution inputs to the air mass factor (AMF). The AMF is a function of the satellite viewing and solar angle, effective cloud radiance fraction and pressure, NO_2 profile shape (generated from the 1° x 1° TM5-MP),[45] and surface albedo (from 0.5° x 0.5° monthly OMI climatologies).[46] We use Level 2 NO_2 tropospheric column densities (VCDs) with a quality descriptor >0.5, cloud fractions <0.3, and solar zenith angles <70°.

Exponentially-Modified Gaussian (EMG) E_{NO_x} Method. NO_x emission rates (E_{NO_x}) can be directly inferred from the downwind *e*-folding distance of urban NO_2 plumes.[30, 34, 47-50] Before calculating E_{NO_x}, we draw a 3° x 3° box centered at each city and remove daily scenes with spatially uneven NO_2 background fields to reduce the influence of biomass burning and soil emissions NO_x emissions, which are large NO_2 sources elevated regionally. (ref) We mask the urban plume as a 0.6° x 0.6° box over the city center and define uneven background fields as days

when mean NO_2 VCDs in any one quadrant are greater than 1 σ the mean over the entire of the 3° x 3° box. To focus on atmospheric conditions in which the downwind NO_2 decay is driven by chemical loss rather than atmospheric dispersion, we remove daily TROPOMI observations when wind speeds are below 3 m s^{-1}. For eleven cities with persistent low wind speed conditions, we relax this threshold to 2 m s^{-1}: Porto Novo, Benin; Bobo Dioulasso, Burkina Faso; Douala, Cameroon; Yaoundé, Cameroon; Libreville, Gabon; Serekunda, Gambia; Takoradi, Ghana; Niamey, Niger; Abuja, Nigeria; Benin City, Nigeria; and Freetown, Sierra Leone. Wind filtering is based on the hourly 10-m wind reanalysis product gridded to 0.25° x 0.25° from the ERA5 produced by the European Centre for Medium-Range Weather Forecasts (ECMWF).[51, 52] Remaining daily images are rotated to a common wind direction and oversampled to 0.01° x 0.01° using a physics-based algorithm that represents individual pixels as sensitivity distributions described by generalized two-dimensional super Gaussian functions.[53]

To calculate E_{NO_x}, we first generate downwind line densities by integrating NO_2 plumes in the across wind direction. Line densities are then fit using an exponentially modified Gaussian (EMG) function (Eq. 1),[50] where α is the plume mass, x_o is the downwind *e*-folding distance, μ_x is plume center relative to the city center, σ_x is the Gaussian width, and B is the line density background. We optimize these parameters using a non-linear curve-fitting programming solver, using the same initial inputs and bounds for each city (Table S1). We calculate the NO_2 effective lifetime ($\tau_{effective}$), equal to the ratio of the optimized x_o and the ERA5 mean wind speed (Eq. 2). Lifetimes determined in this way cannot be treated as true chemical lifetimes, hence they are referred to as 'effective' lifetimes, as they are affected by issues such as grid resolution plume rotation, chemical conversion, plume meandering and sampling choices such as selection of the wind speed

threshold.[32, 33] In Eq. 3, the NO_x emission rate is solved for as the NO_2 plume mass divided by $\tau_{effective}$ and scaled by an NO_x/NO_2 ratio of 1.3.[28]

$$F(x) = \frac{\alpha}{2x_o} \exp\left(\frac{\mu_x}{x_o} + \frac{\sigma_x}{2x_o} - \frac{x}{x_o}\right) \operatorname{erfc}\left(-\frac{1}{\sqrt{2}}\left[\frac{x - \mu_x}{\sigma_x} - \frac{\sigma_x}{x_o}\right]\right) + B \quad (1)$$

$$\tau_{effective} = \frac{x_o}{w} \quad (2)$$

$$E_{NO_x} = 1.3\left(\frac{\alpha}{\tau_{effective}}\right) \quad (3)$$

The uncertainty in E_{NO_x} is computed using the method outline in de Foy, 2015. Here, the uncertainty is calculated as the interquartile range of 100 emission estimates. For each of these estimates, pixels are randomly selected to be included in analysis using a bootstrapping algorithm, prior to any wind rotation or oversampling. The size of the randomly selected data is equal to the original data set. This bootstrapped data set is then processed the same as the original data set, where pixels are rotated to align in a common wind direction and oversampled to 0.01° x 0.01° using a physics-based oversampling. The emissions for the bootstrapped data set is calculated by integrating the NO2 plume in the across wind direction to produce a line density, then fit to the exponentially modified gaussian function (Eq. 1). This process is repeated to produce 100 emission estimates from randomly selected data, and uncertainty is reported as the interquartile range of these estimates.

Flux Divergence E_{NO_x} Method. E_{NO_x} were also computed for urban point sources based on the divergence of the temporal mean NO_2 fluxes and sinks.[35] Here, NO_x fluxes are calculated for U and V components of wind fields. Wind fields used are from hourly ECMWF operational reanalysis ERA5, taken at a vertical model pressure level 975 hPa[54]. Daily wind data from 6-12 UTC is spatially and temporally interpolated to correspond with TROPOMI overpasses. We

calculate the flux by multiplying gridded TROPOMI columns with interpolated wind fields. We then calculate the forth order, first derivative divergence of the fluxes. The divergence approximates the sources, *E,* and sinks, S, of NO_x, shown in Eq 4, where L is a NO_x/NO_2 ratio of 1.3, V is the TROPOMI column, and $\boldsymbol{w}$ is the ERA wind fields. Sinks are approximated from TROPOMI columns, where $S = LV/\tau$, where τ is an average NO_2 lifetime. We calculate emissions and apply a peak fitting algorithm to separate out point sources from residual emissions. This is done by locating the maximum peak in the emission map, which is identified as a peak source. A 2D gaussian is fit around the peak source, and removed from the emission map, yielding the residual emissions. Point source emissions are calculated by taking the sum of the gaussian within the fitting region.

$$E_{NO_x} = D + S = \nabla(LV\mathbf{w}) + LV/\tau \quad (4)$$

We calculate the uncertainty in the point source emissions using the method outlined in Beirle, 2019, where the uncertainty is the quadratic sum of the uncertainty due to peak fitting (20%) and the flux divergence (62%) which is based on uncertainties in *L*(20%), *V*(50%), and *w*(30%). The uncertainty is therefore 65% for point source emissions.

RESULTS AND DISCUSSION

Regional urban NO_x emission rates. We calculate the NO_x emission rates for the following 22 cities, both large and small, in 13 countries (Figure 1, Table 1):Cotonou and Porto Novo, Benin; Ouagadougou and Bobo Dioulasso, Burkina Faso; Yaoundé and Douala, Cameroon; Abidjan, Côte d'Ivoire; Libreville, Gabon; Serekunda and Banjul, The Gambia; Accra and Takoradi, Ghana; Conakry, Guinea; Bamako, Mali; Niamey, Niger; Kano, Lagos, Abuja, and Benin City, Nigeria; Dakar and Kaolack, Senegal; and Freetown, Sierra Leone. Cities were chosen based on criteria

of an NO_2 column that is distinguishable from the background and signal high enough for a confident fit, with strong wind speeds for plume definition, and separation from other major sources.

Emissions are inferred using TROPOMI overpasses and ERA wind fields from May 2018 to February 2020. Emissions for the 22 west African cities ranges from 0.2 to 2.9 Mg hr^{-1}. Average emissions across the cities is 0.7 Mg hr^{-1}. When compared to inventory values, we see a good validation of the line density emissions. There is less agreement between inventory values and flux divergence emissions, due in part by inaccuracies in the EDGAR inventory and the exclusion of background sources in the flux divergence method.

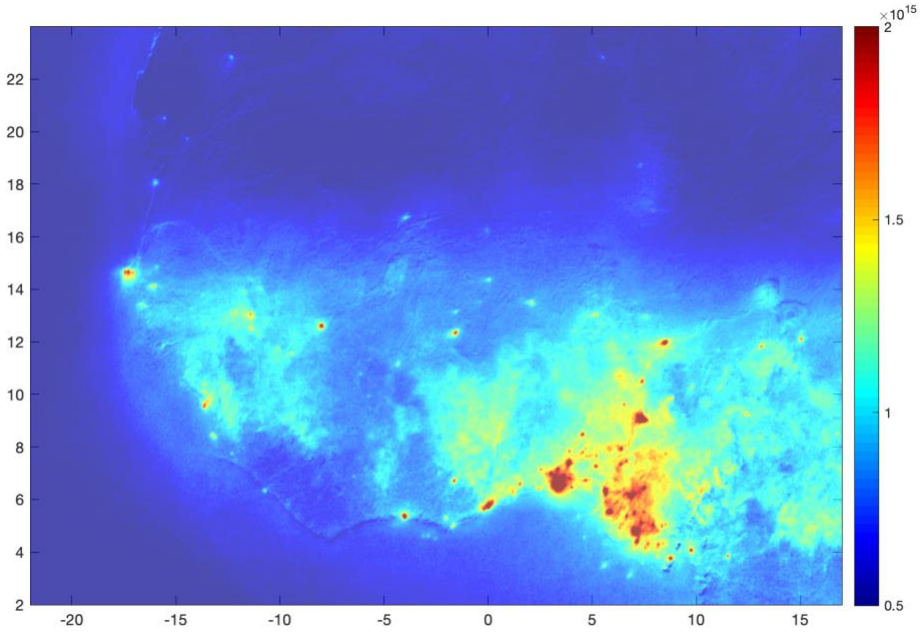

Figure 1. TROPOMI NO_2 VCDs (molecules cm^{-2}) oversampled to 0.01º x 0.01º across West Africa. Observations span May 2018–Feburary 2020.

Using line densities, we infer emission rates for weekdays (defined as Tuesday-Saturday) and Sundays (Figure 2). Four cities had Sunday emissions that were unable to be fit confidently (Table 1); Bobo Dioulasso, Burkina Faso; Yaoundé and Douala, Cameroon; and Libreville, Gabon. We infer emissions for all days to compare with inventory values. Four cities see an increase in emissions weekday to Sunday, all other cities see a decrease. The difference from weekday to Sunday varies for individual cities, but overall we see decrease in emissions from weekdays to Sundays, with an average decrease of 19%, and an average percent difference of 27%.

Table 1. Daytime E_{NO_x} on weekdays and Sundays calculated based on the EMG and flux divergence methods. Annual hourly E_{NO_x} predicted by the EDGAR inventory are also shown.

	Mg Hr^{-1}			
	Line Density Method			**EDGAR**
City	**Weekdays**	**Sundays**	**All days**	**Annual**
Cotonou, Benin	0.2	0.2	0.2 ± 0.02	0.4
Porto Novo, Benin	0.4	0.2	0.4 ± 0.02	0.3
Ouagadougou, Burkina Faso	0.4	0.3	0.4 ± 0.01	0.9
Bobo Dioulasso, Burkina Faso	0.3	-	0.3 ± 0.2	0.3
Yaoundé, Cameroon	0.2	-	0.2 ± 0.1	0.1
Douala, Cameroon	0.4	-	0.4 ± 0.04	0.2
Abidjan, Côte d'Ivoire	0.8	0.5	0.8 ± 0.1	0.9
Libreville, Gabon	0.2	-	0.2 ± 0.1	1.6
Serekunda, Gambia	0.3	0.3	0.3 ± 0.04	0.3
Banjul, The Gambia	0.3	0.2	0.3	0.3
Accra, Ghana	1.6	1.3	1.6 ± 0.1	1.2
Takoradi, Ghana	0.2	0.2	0.2 ± 0.02	0.7
Conakry, Guinea	0.8	0.7	0.8 ± 0.1	0.9
Bamako, Mali	0.5	0.4	0.5 ± 0.02	0.2
Niamey, Niger	0.2	0.2	0.2 ± 0.01	0.2
Benin City, Nigeria	0.5	0.3	0.5 ± 0.2	1
Kano, Nigeria	0.8	0.8	0.8 ± 0.01	1.2
Lagos, Nigeria	2.9	3.0	2.9 ± 0.1	2.9
Abuja, Nigeria	1.0	0.3	0.9 ± 0.2	1.2

Dakar, Senegal	1.5	1.2	1.4 ± 0.02	2.2
Kaolack, Senegal	0.3	0.3	0.3 ± 0.02	0.2
Freetown, Sierra Leone	0.3	0.6	0.3 ± 0.01	0.5

We compared inferred line density emissions for all days to reported values in the Emissions Database for Global Atmospheric Research (EDGAR) inventory[55] (Table 1). Regionally we see good agreement between the inventory and our emission estimates, with some larger discrepancies for individual cities, and a mean percentage difference of 40%. The EDGAR inventory was last released in 2015 and is well known to not be well constrained for regions lacking observations, such as West Africa. Based on the errors associated with satellite measurements as well as with EDGAR estimates, this comparison is a good validation of our inferred line density emissions.

NO_x emissions in Dakar, Senegal. Dakar is the capital and largest city in Senegal, which, while isolated from other major urban centers, is a composite of multiple NO_2 plumes over Dakar city, the Industrial Zone, and Blaise Diagne International Airport (DSS). These plumes are connected by a transportation corridor and various suburban areas, including Pikine and Rufisque (Figure 3a). During the dry season, there are generally two types of prevailing winds: the northwest marine trade winds, originating in the Azores anticyclone and bringing unpolluted maritime air to the Cap Vert Peninsula, and the continental trade winds, or Harmattan, originating in the north Saharan anticyclone[56] and bringing hot, dry, and dust-enriched air masses to the region.[57] During the rainy season, airflows are controlled by the positioning of the intertropical convergence zone, with convergence of northwest and northeast trade winds and the southwest monsoon occurring over Senegal and typically leading to the inflow of cool, humid, maritime air to the Cap Vert Peninsula.[56] When NO_2 TVCDs are sorted (not rotated) for all dry and wet season days with northerly surface winds (defined as –35° to 35°), at least three major plumes become distinct and

non-urban biomass-burning influences are simultaneously minimized (Figure 3b). Here, we take advantage of these airflow conditions to separately compute NO_x emission rates for Dakar city, the Industrial Zone, and DSS based on Eqs. 1–3, comparing results with NO_x fluxes determined using Eq. 4.

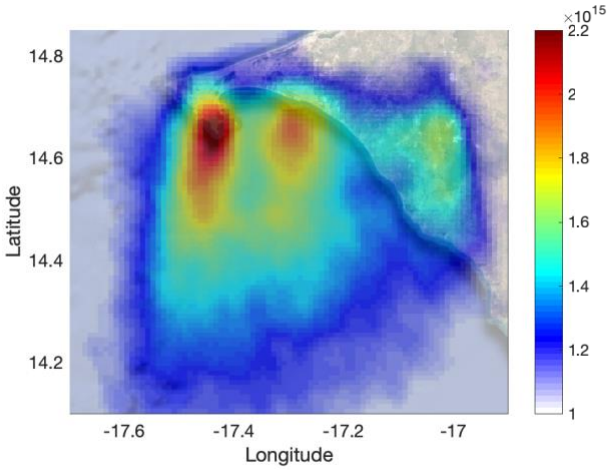

Figure 3. NO_2 TVCDs (molecules cm^{-2}) over Dakar, Senegal from May 2018 to February 2020 oversampled to 0.01° x 0.01° weekdays with northerly surface wind conditions only. Background map data: Landsat 8 composite, May 2018–February 2020.

Before calculating E_{NO_x} by Eqs. 1–3, we separate the three plumes. For each cross section, prior to integrating the line densities we fit the three major sources with a Gaussian curve. In this approach, cross sections may lead to emission rates that are over or underestimated when plume shapes are asymmetrical or when initial fitting guesses cannot be identified algorithmically, as they must be forced, which is done using the last previously identified values.

E_{NO_x} are reported for weekdays and Sundays over June 2018–February 2021 (Table 2). On weekdays, the city of Dakar is the largest source of NO_x in full urban area, followed by the

Industrial Zone and DSS, respectively. Vehicle traffic is a major NO_x source within the Dakar city plume,[13, 58] comprised of new and used personal vehicles (largely diesel powered), two-wheeled vehicles, public and shared transportation vehicles such as Car Rapides, Ndiaga Ndiaye buses, and Tatas, and heavy-duty diesel trucks that primarily transport goods to and from the Port of Dakar. Local regulations stipulate that heavy-duty diesel trucks operate at night only; therefore, their influence on daytime NO_x emission rates is limited to next-day NO_2 carryover. Other NO_x sources include supplemental diesel generator exhaust, shipping emissions, and other forms of home and commercial combustion.[13] Traffic in the city of Dakar is visibly reduced on Sundays compared to weekdays, with E_{NO_x} reductions of 32% on Sundays and weekday-Sunday decreases in NO and NO_2 mixing ratios having been previously reported.[13] At the same time, smaller weekday-Sunday decreases are observed in the Industrial Zone, where emissions are dominated by manufacturing activities and electricity generation, which generally do not exhibit significant weekday-Sunday differences. The largest weekday-Sunday changes in emissions are observed over DSS, where NO_x emission rates are more than 65% lower on Sundays. We examine emissions of April – June 2020, when the city of Dakar was in lockdown and flights to and from DSS were restricted. We compare this to the same time period in 2019, when activities are not restricted. We see a large decrease in emissions over from 2019 to 2020, with a 55% difference in emissions using the spectral separation and 21% difference in emissions using the baseline division. This indicates that the emissions over the DSS are primarily controlled by emissions from the airport.

Table 2. Daytime E_{NO_x} on weekdays (Tuesday–Saturday) and Sundays based on Eqs. 1–3, with plumes separated spectrally and using Eq. 4. For all estimates, E_{NO_x} are computed for days with northerly surface wind conditions only (–35° to 35°) over May 2018–February 2020.

	Spectrally Separated		
	Weekdays (Mg h^{-1})	Sundays (Mg h^{-1})	Percent difference
Total Plume	1.4 ± 0.5	1.1 ± 0.4	24
Dakar	0.4 ± 0.1 (35%)	0.3 ± 0.1 (30%)	32
Industrial Zone	0.3 ± 0.1 (25%)	0.3 ± 0.1 (30%)	20
Airport	0.4 ± 0.1 (20%)	0.2 ± 0.1 (20%)	65
	Flux Divergence		
	Weekdays (Mg h^{-1})	Sundays (Mg h^{-1})	Percent difference
Total Plume	1.4 ± 0.5	1.1 ± 0.4	24
Dakar	0.4 ± 0.1 (35%)	0.3 ± 0.1 (30%)	32
Industrial Zone	0.3 ± 0.1 (25%)	0.3 ± 0.1 (30%)	20
Airport	0.4 ± 0.1 (20%)	0.2 ± 0.1 (20%)	65

For comparison, we calculate E_{NO_x} from the NO_2 flux divergence fields (Eq. 4), which also resolve three major sources within the full urban area (Figure 3d). Likewise, on weekdays, the city of Dakar is the largest source of NO_x emissions followed by the Industrial Zone and DSS. NO_x emissions in Dakar city are calculated to decrease by 29% on weekdays compared to Sundays, with 29% lower emission rates in the Industrial Zone on Sundays than weekdays. Similarly, we find large weekday-Sunday reductions in NO_x emissions over DSS.

Conclusion. We infer emissions in 22 West African cities using two different methods. By comparing these two methods we can yield more accurate emission estimates for an understudied region. These can be used to improve our understanding of atmospheric conditions in West Africa. We examine trends in emissions from weekdays to Sundays. This can yield information about the

surface chemistry and pollution sources in these cities. Across all cities we generally see a decrease in emissions from weekdays to Sundays.

While the magnitude of emissions in the two methods are not entirely consistent, the two methods do produce the same patterns for most cities, and the differences in the methods are within their uncertainties. Emission estimates from both methods can be used to further elucidate local surface chemistry in these cities. The difference between these methods and inventory values can be examined and used to improve inventories in the future, and can be used to adjust model inputs for the region.

We advance previous methods by examining areas with overlapping plumes, and we develop two methods to estimate individual sources. This allows for the method to be applied in areas that would previously be excluded from analysis. This development in the method allows for cities with more diverse pollution sources to be examined, and extends the practical use of a developed method.

Acknowledgments. This research was funded by the University of Virginia Environmental Resilience Institute and an NSF CAREER Award (AGS 2047150) to SEP. MAM was supported by the Virginia Space Grant Consortium Graduate Fellowship Program. AF acknowledges support from the African Institute for Mathematical Sciences Next Einstein Initiative Women's Fellowship in Climate Change Science. TROPOMI NO_2 Level 2 vertical column densities are publicly accessible at https://earthdata.nasa.gov/earth-observation-data. The EDGAR emission inventory (EC-JRC/PBL) is available at http://edgar.jrc.ec.europa.eu. ERA5 reanalysis wind fields are produced by the European Centre for Medium-Range Weather Forecasts (ECWMF) and can be freely downloaded from the Climate Data Store (https://cds.climate.copernicus.eu/). Local

Meteorological Terminal Air Report (METAR) reports can be downloaded at ogimet.com/metars.phtml.

References

1. Zhu, T.; Melamed, M. L.; Parrish, D.; Gauss, M.; Klenner, L. G.; Mark Lawrence; Konare, A.; Liousse, C. *WMO/IGAC Impacts of Megacities on Air Pollution and Climate*; World Meteorological Organization: 2012.
2. Hickman, J. E.; Andela, N.; Tsigaridis, K.; Galy-Lacaux, C.; Ossohou, M.; Bauer, S. E., Reductions in NO₂ burden over north equatorial Africa from decline in biomass burning in spite of growing fossil fuel use, 2005 to 2017. *Proceedings of the National Academy of Sciences* **2021,** *118* (7), e2002579118.
3. Roy, R., The cost of air pollution in Africa. **2016**.
4. Heft-Neal, S.; Burney, J.; Bendavid, E.; Burke, M., Robust relationship between air quality and infant mortality in Africa. *Nature* **2018,** *559* (7713), 254-258.
5. Cobbinah, P. B.; Erdiaw-Kwasie, M. O.; Amoateng, P., Africa's urbanisation: Implications for sustainable development. *Cities* **2015,** *47*, 62-72.
6. Dodman, D.; Leck, H.; Rusca, M.; Colenbrander, S., African Urbanisation and Urbanism: Implications for risk accumulation and reduction. *International Journal of Disaster Risk Reduction* **2017,** *26*, 7-15.
7. Liousse, C.; Assamoi, E.; Criqui, P.; Granier, C.; Rosset, R., Explosive growth in African combustion emissions from 2005 to 2030. *Environmental Research Letters* **2014,** *9* (3).
8. Bahino, J.; Véronique, Y.; Corinne, G.-L.; Adon, M.; Aristide, A.; Keita, S.; Liousse, C.; Gardrat, E.; Chiron, C.; Ossohou, M.; Gnamien, S.; Djossou, J., A pilot study of gaseous pollutants' measurement (NO₂, SO₂, NH₃, HNO₃ and O₃) in Abidjan, Côte d'Ivoire: contribution to an overview of gaseous pollution in African cities. *Atmospheric Chemistry and Physics* **2018,** *18*, 5173-5198.
9. Ngom, B.; Seye, M. R.; Diallo, M.; Gueye, B.; Drame, M. S. In *A Hybrid Measurement Kit for Real-time Air Quality Monitoring Across Senegal Cities*, 2018 1st International Conference on Smart Cities and Communities (SCCIC), 24-26 July 2018; 2018; pp 1-6.
10. Baskin, A. *Africa Used Vehicle Report*; 2018.
11. Kumar, A. B., F., Stuck in Traffic: Urban Transport in Africa. AICD Background Paper 2008; Vol. Vol. 1.
12. Osuntogun, B.; C.A, K., Environmental-impacts of Urban Road Transportation in South-western States of Nigeria. *Journal of Applied Sciences* **2007,** *7*.
13. Adon, M.; Yoboué, V.; Galy-Lacaux, C.; Liousse, C.; Diop, B.; Doumbia, E. H. T.; Gardrat, E.; Ndiaye, S. A.; Jarnot, C., Measurements of NO2, SO2, NH3, HNO3 and O3 in West African urban environments. *Atmospheric Environment* **2016,** *135*, 31-40.
14. Nanaa, B.; Sanogob, O.; Savadogoa, P. W.; Dahoa, T.; Boudad, M.; Koulidiatia, J., Air Quality Study in Urban Centers: Case Study of Ouagadougou, Burkina Faso. *FUTY Journal of the Environment* **2012,** *7*, 1-18.

15. Ibe, F. C.; Njoku, P. C.; Alinnor, J. I.; Opara, A. I., SPATIAL VARIATION OF NO2 AND SO2 IN THE AMBIENT
ENVIRONMENT OF IMO STATE, NIGERIA. *International Journal of Science, Environment and Technology*
2016, *5* (1), 33-46.
16. Ibe, F. C.; Njoku, P. C.; Alinnor Jude, I.; Opara, A. I., Evaluation of Ambient Air quality in parts of Imo state, Nigeria. *Research Journal of Chemical Sciences* **2016,** *6* (1), 41-52.
17. Ibe, F. C.; Opara, A. I.; Duru, C. E.; Obinna, I. B.; Enedoh, M. C., Statistical analysis of atmospheric pollutant concentrations in parts of Imo State, Southeastern Nigeria. *Scientific African* **2020,** *7*, e00237.
18. Arku, R. E.; Vallarino, J.; Dionisio, K. L.; Willis, R.; Choi, H.; Wilson, J. G.; Hemphill, C.; Agyei-Mensah, S.; Spengler, J. D.; Ezzati, M., Characterizing air pollution in two low-income neighborhoods in Accra, Ghana. *Science of The Total Environment* **2008,** *402* (2), 217-231.
19. Mama, D.; Dimon, B.; Aina, M.; Adounkpe, J.; Ahomadegbe, M.; Youssao, A.; Kouazounde, J.; Pedro Kouanda, S.; Moudachirou, M., Transport urbain au Benin et pollution atmosphérique: évaluation quantitative de certains polluants chimiques de Cotonou. **2013,** *7* (1), 377-386.
20. Obanijesu, E. O.; Adebiyi, F. M.; Sonibare, J. A.; Okelana, O. A., Air-borne SO2 Pollution Monitoring in the Upstream Petroleum Operation Areas of Niger-Delta, Nigeria. *Energy Sources, Part A: Recovery, Utilization, and Environmental Effects* **2009,** *31* (3), 223-231.
21. Coker, E.; Kizito, S., A Narrative Review on the Human Health Effects of Ambient Air Pollution in Sub-Saharan Africa: An Urgent Need for Health Effects Studies. *International Journal of Environmental Research and Public Health* **2018,** *15* (3), 427.
22. Jaeglé, L.; Steinberger, L.; Martin, R. V.; Chance, K., Global partitioning of NOx sources using satellite observations: relative roles of fossil fuel combustion, biomass burning and soil emis- sions. Faraday Discussions: 2005; Vol. 130, pp 407-23
23. Lamsal, L. N.; Martin, R. V.; A. Padmanabhan, A.; A. van Donkelaar, A.; Q. Zhang, Q.; C. E. Sioris, C. E.; K., K. C.; T. P. Kurosu, T. P.; Newchurch, M. J., Application of satellite observations for timely updates to global anthropogenic NOx emission inventories. Geophysical Research Letters: 2011; Vol. 38.
24. Martin, R. V.; Jacob, D. J.; Chance, K.; Kurosu, T. P.; Palmer, P. I.; Evans, M. J., Global inventory of nitrogen oxide emis- sions constrained by space-based observations of NO2 columns,. Journal of Geophysical Research 2003; Vol. 108, p 4537.
25. Geddes, J. A.; Martin, R. V.; Boys, B. L.; van Donkelaar, A., Long-Term Trends Worldwide in Ambient NO2 Concentrations Inferred from Satellite Observations. *Environmental Health Perspectives* **2016,** *124* (3), 281-289.
26. Veefkind, J. P.; Aben, I.; McMullan, K.; Förster, H.; de Vries, J.; Otter, G.; Claas, J.; Eskes, H. J.; de Haan, J. F.; Kleipool, M.; al., e., TROPOMI on the ESA Sentinel-5 Precursor: A GMES Mission for Global Observations of the Atmospheric Composition for Climate , Air Quality and Ozone Layer Applications. Remote Sensing Environment: 2012; Vol. 120, pp 70-83.
27. Krotkov, N. A.; McLinden, C. A.; Li, C.; Lamsal, L. N.; Celarier, E. A.; Marchenko, S. V.; Swartz, W. H.; Bucsela, E. J.; Joiner, J.; Duncan, B. N.; Boersma, K. F.; Veefkind, J. P.; Levelt, P. F.; Fioletov, V. E.; Dickerson, R. R.; He, H.; Lu, Z.; Streets, D. G., Aura OMI observations of

regional SO2 and NO2 pollution changes from 2005 to 2015. *Atmos. Chem. Phys.* **2016,** *16* (7), 4605-4629.
28. Beirle, S.; Boersma, K. F.; Platt, U.; Lawrence, M. G.; Wagner, T., Megacity emissions and lifetimes of nitrogen oxides probed from space. *Science* **2011,** *333* (6050), 1737-9.
29. Valin, L. C.; Russell, A. R.; Cohen, R. C., Variations of OH radical in an urban plume inferred from NO2 column measurements. Geophysical Research Letters: 2013; Vol. 40, pp 1856-1860.
30. de Foy, B.; Lu, Z.; Streets, D. G.; Lamsal, L. N.; Duncan, B. N., Estimates of power plant NOx emissions and lifetimes from OMI NO2 satellite retrievals. Atmospheric Environment: 2015; Vol. 116, pp 1-11.
31. Goldberg, D. L.; Lu, Z.; Streets, D. G.; de Foy, B.; Griffin, D.; McLinden, C. A.; Lamsal, L. N.; Krotkov, N. A.; Eskes, H., Enhanced Capabilities of TROPOMI NO. *Environ Sci Technol* **2019,** *53* (21), 12594-12601.
32. Lu, Z.; Streets, D. G.; de Foy, B.; Lamsal, L. N.; Duncan, B. N.; Xing, J., Emissions of nitrogen oxides from US urban areas: es- timation from Ozone Monitoring Instrument retrievals for 2005– 2014. Atmospheric Chemistry and Physics: 2015; Vol. 15, pp 10367-10383.
33. Laughner, J. L.; Cohen, R. C., Direct observation of changing NO. *Science* **2019,** *366* (6466), 723-727.
34. Liu, F.; Beirle, S.; Zhang, Q.; Dörner, S.; He, K.; Wagner, T., NOx Lifetimes and Emissions of Cities and Power Plants in Polluted Background Estimated by Satellite Observations. Atmospheric Chemistry and Physics: 2016; Vol. 16, pp 5283-5298.
35. Beirle, S.; Borger, C.; Dörner, S.; Li, A.; Hu, Z.; Liu, F.; Wang, Y.; Wagner, T., Pinpointing nitrogen oxide emissions from space. *Sci Adv* **2019,** *5* (11), eaax9800.
36. Crippa, M.; Guizzardi, D.; Muntean, M.; Schaaf, E., EDGAR v5.0 Global Air Pollutant Emissions. European Commission. (JRC), J. R. C., Ed. 2019.
37. van Geffen, J. H. G.; Boersma, K. F.; Eskes, H. J.; Maasakkers, J. D.; Veefkind, J. P. TROPOMI ATBD of the total and tropospheric NO2 data products. http://www.tropomi.eu (accessed 12 May).
38. Veefkind, J. P.; Aben, I.; McMullan, K.; Förster, H.; de Vries, J.; Otter, G.; Claas, J.; Eskes, H. J.; de Haan, J. F.; Kleipool, Q.; van Weele, M.; Hasekamp, O.; Hoogeveen, R.; Landgraf, J.; Snel, R.; Tol, P.; Ingmann, P.; Voors, R.; Kruizinga, B.; Vink, R.; Visser, H.; Levelt, P. F., TROPOMI on the ESA Sentinel-5 Precursor: A GMES mission for global observations of the atmospheric composition for climate, air quality and ozone layer applications. *Remote Sensing of Environment* **2012,** *120*, 70-83.
39. Boersma, K. F.; Eskes, H. J.; Dirksen, R. J.; van der A, R. J.; Veefkind, J. P.; Stammes, P.; Huijnen, V.; Kleipool, Q. L.; Sneep, M.; Claas, J.; Leitão, J.; Richter, A.; Zhou, Y.; Brunner, D., An improved tropospheric NO₂ column retrieval algorithm for the Ozone Monitoring Instrument. *Atmos. Meas. Tech.* **2011,** *4* (9), 1905-1928.
40. Lorente, A.; Folkert Boersma, K.; Yu, H.; Dörner, S.; Hilboll, A.; Richter, A.; Liu, M.; Lamsal, L. N.; Barkley, M.; De Smedt, I.; Van Roozendael, M.; Wang, Y.; Wagner, T.; Beirle, S.; Lin, J. T.; Krotkov, N.; Stammes, P.; Wang, P.; Eskes, H. J.; Krol, M., Structural uncertainty in air mass factor calculation for NO2 and HCHO satellite retrievals. *Atmos. Meas. Tech.* **2017,** *10* (3), 759-782.

41. van Geffen, J. H. G. M.; Boersma, K. F.; Van Roozendael, M.; Hendrick, F.; Mahieu, E.; De Smedt, I.; Sneep, M.; Veefkind, J. P., Improved spectral fitting of nitrogen dioxide from OMI in the 405–465 nm window. *Atmos. Meas. Tech.* **2015,** *8* (4), 1685-1699.
42. Zara, M.; Boersma, K. F.; De Smedt, I.; Richter, A.; Peters, E.; van Geffen, J. H. G. M.; Beirle, S.; Wagner, T.; Van Roozendael, M.; Marchenko, S.; Lamsal, L. N.; Eskes, H. J., Improved slant column density retrieval of nitrogen dioxide and formaldehyde for OMI and GOME-2A from QA4ECV: intercomparison, uncertainty characterisation, and trends. *Atmos. Meas. Tech.* **2018,** *11* (7), 4033-4058.
43. Boersma, K. F.; Eskes, H. J.; Richter, A.; De Smedt, I.; Lorente, A.; Beirle, S.; van Geffen, J. H. G. M.; Zara, M.; Peters, E.; Van Roozendael, M.; Wagner, T.; Maasakkers, J. D.; van der A, R. J.; Nightingale, J.; De Rudder, A.; Irie, H.; Pinardi, G.; Lambert, J. C.; Compernolle, S. C., Improving algorithms and uncertainty estimates for satellite NO2 retrievals: results from the quality assurance for the essential climate variables (QA4ECV) project. *Atmos. Meas. Tech.* **2018,** *11* (12), 6651-6678.
44. Judd, L. M., Evaluating Sentinel-5P TROPOMI tropospheric NO2 column densities with airborne and Pandora spectrometers near New York City and Long Island Sound. Atmospheric Measurement Techniques: 2020; Vol. 13, pp 6113–6140.
45. Williams, J. E.; Boersma, K. F.; Le Sager, P.; Verstraeten, W. W., The high-resolution version of TM5-MP for optimized satellite retrievals: description and validation. *Geosci. Model Dev.* **2017,** *10* (2), 721-750.
46. Kleipool, Q. L.; Dobber, M. R.; de Haan, J. F.; Levelt, P. F., Earth surface reflectance climatology from 3 years of OMI data. *J. Geophys. Res.-Atmos.* **2008,** *113* (D18).
47. Beirle, S.; Boersma, K. F.; Platt, U.; Lawrence, M. G.; Wagner, T., Megacity Emissions and Lifetimes of Nitrogen Oxides Probed from Space. *Science* **2011,** *333* (6050), 1737-1739.
48. Valin, L. C.; Russell, A. R.; Cohen, R. C., Variations of OH radical in an urban plume inferred from NO2 column measurements. *Geophys. Res. Lett.* **2013,** *40* (9), 1856-1860.
49. Goldberg, D. L.; Lu, Z.; Streets, D. G.; de Foy, B.; Griffin, D.; McLinden, C. A.; Lamsal, L. N.; Krotkov, N. A.; Eskes, H., Enhanced Capabilities of TROPOMI NO2: Estimating NOX from North American Cities and Power Plants. *Environ. Sci. Technol.* **2019**.
50. Laughner, J. L.; Cohen, R. C., Direct observation of changing NO_x lifetime in North American cities. *Science* **2019,** *366* (6466), 723-727.
51. Valor, G. B. *Ogimet*. ogimet.com/metars.phtml.
52. Hersbach, H.; Bell, B.; Berrisford, P.; Biavati, G.; Horányi, A.; Muñoz Sabater, J.; Nicolas, J.; Peubey, C.; Radu, R.; Rozum, I.; Schepers, D.; Simmons, A.; Soci, C.; Dee, D.; Thépaut, J.-N., ERA5 hourly data on single levels from 1979 to present. (CDS)., C. C. C. S. C. S. C. D. S., Ed. 2018.
53. Sun, K.; Zhu, L.; Cady-Pereira, K.; Chan Miller, C.; Chance, K.; Clarisse, L.; Coheur, P. F.; González Abad, G.; Huang, G.; Liu, X.; Van Damme, M.; Yang, K.; Zondlo, M., A physics-based approach to oversample multi-satellite, multispecies observations to a common grid. *Atmos. Meas. Tech.* **2018,** *11* (12), 6679-6701.
54. Hersbach, H.; Bell, B.; Berrisford, P.; Biavati, G.; Horányi, A.; Muñoz Sabater, J.; Nicolas, J.; Peubey, C.; Radu, R.; Rozum, I.; Schepers, D.; Simmons, A.; Soci, C.; Dee, D.; Thépaut, J.-N., ERA5 hourly data on pressure levels from 1979 to present. . Copernicus Climate Change Service (C3S) Climate Data Store (CDS): 2018.

55. (PBL), E. C. E. J. R. C. J. N. E. A. A., Emission Database for Global Atmospheric Research (EDGAR), release EDGAR v5.0 (1970 – 2015) of April 2020.
56. Fall, S.; Niyogi, D.; Semazzi, F. H. M., Analysis of Mean Climate Conditions in Senegal (1971–98). *Earth Interactions* **2006,** *10* (5), 1-40.
57. Sow, B.; Tchanche, B.; Fall, I.; Souaré, S.; Mbow-Diokhané, A., Monitoring of Atmospheric Pollutant Concentrations in the City of Dakar, Senegal. *Open Journal of Air Pollution* **2021,** *10*, 18-30.
58. Sarr, D.; Diop, B.; Farota, A. K.; Sy, A.; Diop, A. D.; Wade, M.; Diop, A. B., Atmospheric Circulation in Low Troposphere-Effect On NOx and CO Emissions in Traffic and Air Quality in Dakar. *Journal of Pollution Effects & Control* **2018,** *6*, 1–14.